

## Corrosion inhibition performance of 5-(2-hydroxyethyl)-1,3,5-triazine-2-thione for 10# carbon steel in NH<sub>4</sub>Cl solution

Chengxian Yin<sup>1,2</sup>, Xiling Ban<sup>3</sup>, Yuan Wang<sup>1,2</sup>, Juantao Zhang<sup>1,2</sup>, Lei Fan<sup>1,2</sup>, Rui Cai<sup>1,2</sup>, Junping Zhang<sup>3,\*</sup>

<sup>1</sup> State Key Laboratory for Performance and Structure Safety of Petroleum Tubular Goods and Equipment Materials, Xi'an 710077, China

<sup>2</sup> CNPC Tubular Goods Research Institute, Xi'an 710077, China

<sup>3</sup> Department of Applied Chemistry, School of Natural and Applied Science, Northwestern Polytechnical University, Xi'an 710072, China

\*E-mail: [zhangjunping@nwpu.edu.cn](mailto:zhangjunping@nwpu.edu.cn)

Received: 23 June 2019 / Accepted: 11 October 2019 / Published: 29 October 2019

---

In this work, 5-(2-hydroxyethyl)-1,3,5-triazine-2-thione (HOTAT) was synthesized, and its chemical structure was characterized using FTIR and <sup>1</sup>H NMR. The corrosion inhibition performance of HOTAT for 10# carbon steel in 2% NH<sub>4</sub>Cl solution was studied by weight loss and electrochemical methods. The results showed that HOTAT is a good corrosion inhibitor for 10# carbon steel in 2% NH<sub>4</sub>Cl solution. The inhibition efficiency of HOTAT increases with increasing inhibitor concentration and decreases with the temperature. The results obtained from potentiodynamic polarization experiments indicate that HOTAT behaves as a mixed-type inhibitor. The adsorption of HOTAT on the 10# carbon steel surface obeys the Langmuir adsorption isotherm, and its adsorption is spontaneous and exothermic.

---

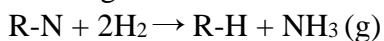
**Keywords:** Corrosion inhibitor; Synthesis; Electrochemical; Adsorption isotherm

### 1. INTRODUCTION

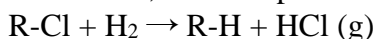
Metal materials are often damaged or degraded by the environment during use. Thermodynamic studies have shown that metal corrosion is spontaneous and unavoidable. Corrosion not only leads to the waste of metal resources but also causes corrosion damage to metal structures, which results in large economic losses and catastrophic accidents and depletes noble energy and resources. Of all possible anti-corrosion measures, the use of a corrosion inhibitor is one of the most economic and effective methods for reducing metal corrosion [1-3]. After decades of efforts, great progress has been made in the development and research of corrosion inhibitors, and many types of corrosion inhibitors have been developed [4-8]. Due to environmental protection requirements, high efficiency and low toxicity are

driving the development of corrosion inhibitors, and many “green corrosion inhibitors” have been developed [9-12] in recent years. Currently, most research focuses on corrosion inhibitors for inorganic acid corrosion [13-15], organic acid corrosion [16-18], salt solution corrosion [19-21] and alkaline corrosion [22-24].

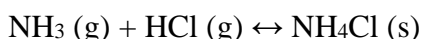
In the oil refinery industry, ammonium chloride ( $\text{NH}_4\text{Cl}$ ) corrosion has been reported to be one of the main causes of equipment and piping failures [25-27]. The hydrogenation of hydrocarbons with  $\text{H}_2$  is used to saturate olefins and remove impurities [28]. Hydrodenitrogenation is performed according to the following exothermic reaction:



In addition, chloride production can occur via reactions such as:



In gaseous streams containing  $\text{NH}_3$  and  $\text{HCl}$ , acid salts can precipitate according to the following reversible reaction:



The solid  $\text{NH}_4\text{Cl}$  can be deposited on the surface of the equipment and cause serious under-deposit corrosion. Water injection processes are often used to dissolve  $\text{NH}_4\text{Cl}$  deposits to minimize under-deposit corrosion. However,  $\text{NH}_4\text{Cl}$  can be hydrolyzed to form a strong acid, which can create an active-passive cell and leads to pitting, crevice corrosion or corrosion cracking. To date, most corrosion inhibitor studies mainly focused on Zn corrosion in  $\text{NH}_4\text{Cl}$  solutions [29-30], which are usually used in batteries. Few investigations of carbon steel inhibitors in  $\text{NH}_4\text{Cl}$  solutions have been reported.

The aim of this study is to synthesize 5-(2-hydroxyethyl)-1,3,5-triazine-2-thione (HOTAT) as a corrosion inhibitor for 10# carbon steel in 2%  $\text{NH}_4\text{Cl}$  solution. The corrosion inhibition action of HOTAT was evaluated by weight loss, polarization and electrochemical impedance spectroscopy (EIS) techniques. Furthermore, the inhibitor adsorption mechanism on the mild steel surface was evaluated by determining the thermodynamic parameters.

## 2. EXPERIMENTAL

### 2.1. Instruments and agents

Thiourea, formaldehyde and monoethanolamine were obtained from Sinopharm Chemical Reagent Co., Ltd. (Shanghai, P.R. China). All the chemicals in this study were analytical reagent grade. The instruments used in this work included an AVATAR-360 Fourier transform infrared (FTIR) spectrometer, AVANCE 800 nuclear magnetic resonance spectrometer and JSM 5600LV scanning electron microscope (SEM).

### 2.2. Synthesis of HOTAT

The synthesis route of HOTAT is shown in Fig. 1.

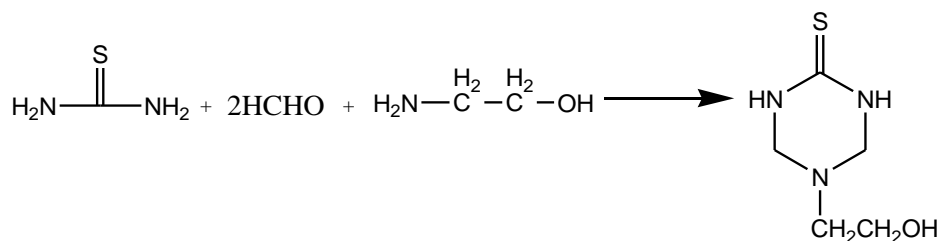


**Figure 1.** Synthesis route of HOTA

Monoethanolamine was added to a mixture of thiourea and 37% aqueous formaldehyde in a molar ratio of 1:1:2 in a three-necked flask at ambient temperature. Then, the mixture was heated to 70 °C and stirred for two hours. After cooling, it was filtered to give a white solid compound, which was identified as the title compound using FTIR and <sup>1</sup>H NMR.

### 2.3. Weight loss experiments

The specimens used in the weight loss experiments were 10# carbon steel with the following composition in wt. %: C: 0.097, Si: 0.206, Mn: 0.413, P: 0.017, S: 0.007, Ni: 0.004, Cr: 0.019, Mo: 0.002, V: 0.001, Cu: 0.004 and Fe: the balance. The dimensions of the rectangular specimen were 5.0 cm × 1.0 cm × 0.3 cm. The surface of the specimen was polished with silicon carbide paper up to 800 grit, rinsed with distilled water and degreased with acetone before each experiment. The corrosive media were NH<sub>4</sub>Cl solutions with different concentrations, which were prepared using NH<sub>4</sub>Cl and distilled water. All the experiments were conducted at 50-80 °C for 6 hours. The specimens were recovered from the solution, and the corrosion product was eliminated using a film-removing solution. Then, the specimens were rinsed with distilled water, degreased with acetone, dried and weighed. The corrosion rate (*v*) and inhibition efficiency (*IE<sub>w</sub>*) were calculated according to equations (1) and (2) [31-33], respectively.

$$v = \frac{8.76 \times 10^4 \times \Delta m}{\rho \times t \times S} \quad (1)$$

where *v* (mm/a) is the corrosion rate of the steel,  $\Delta m$  (g) is the weight loss of the steel,  $\rho$  (g/cm<sup>3</sup>) is the density of the steel, *t* (h) is the immersion time, and *S* (cm<sup>2</sup>) is the surface area of the specimen.

$$IE_w = \frac{v_0 - v}{v_0} \times 100 \quad (2)$$

where *v*<sub>0</sub> and *v* are the corrosion rates of steel in the absence and presence of the corrosion inhibitor.

### 2.4. Electrochemical experiments

Potentiodynamic polarization curves and electrochemical impedance spectra were obtained using a CorrTest instrument (CS350, China). The experiments were performed using a standard three-electrode cell. A steel cylinder inside a Teflon holder served as the working electrode, which had a working area of 1.00 cm<sup>2</sup>. A graphite rod was used as the counter electrode, and a saturated calomel electrode (SCE)

served as the reference electrode. The polarization curves were recorded from -150 to 200 mV vs. the corrosion potential ( $E_{corr}$ ) with a sweep rate of 0.5 mV/s, and the electrochemical impedance spectra were obtained between 100 kHz and 10 mHz.

The  $IE_i$  (%) values were calculated from the potentiodynamic pol

arization measurements using equation (3) [34-35]:

$$IE_i = \frac{I_{corr} - I'_{corr}}{I_{corr}} \times 100 \quad (3)$$

where  $I_{corr}$  and  $I'_{corr}$  are the corrosion currents in the absence and presence of the corrosion inhibitor, respectively.

### 3. RESULTS AND DISCUSSION

#### 3.1. FTIR analysis of the synthesized product

Fig. 2 shows the Fourier transform infrared spectrum of the synthesized product.

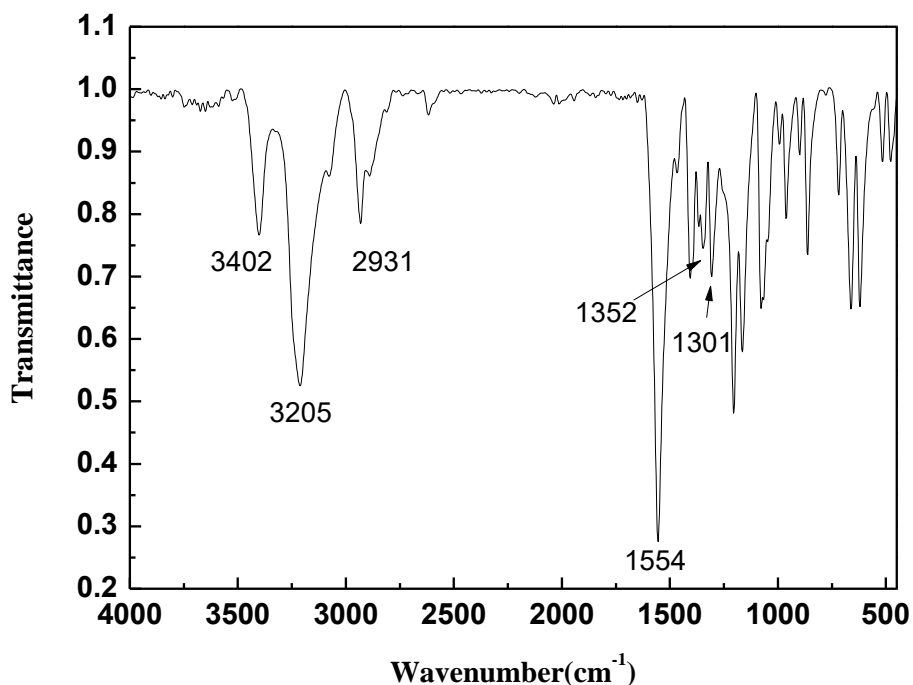


**Figure 2.** FTIR spectrum of the product

The peak at  $3402\text{ cm}^{-1}$  was attributed to the stretching vibration of  $-\text{OH}$ . The peak at  $3205\text{ cm}^{-1}$  was due to the stretching vibration of  $-\text{NH}-$ . The peak at  $2931\text{ cm}^{-1}$  was attributed to the aliphatic symmetric stretching of  $\text{CH}$ . The peak at  $1554\text{ cm}^{-1}$  was due to the bending vibration of  $-\text{NH}-$ . The peak at  $1352\text{ cm}^{-1}$  corresponded to the stretching vibration of  $\text{C-N}$ . The peak at  $1301\text{ cm}^{-1}$  appeared due to the frequency doubling and combined frequencies of the stretching and deformation vibrations of  $\text{C=S}$ .

### 3.2. $^1\text{H}$ NMR analysis of the synthesized product

To confirm the structure of the product,  $^1\text{H}$  NMR spectroscopy was performed. The  $^1\text{H}$  NMR spectrum of the product exhibited bands at  $\delta=8.03$  ppm (s, 2H, -NH-),  $\delta=4.59\text{--}4.57$  ppm (m, 1H, -OH),  $\delta=4.02$  ppm (s, 4H,  $\text{NH-CH}_2\text{-N-CH}_2\text{-NH}$ ),  $\delta=3.51\text{--}3.54$  ppm (m, 2H,  $\text{NCH}_2\text{CH}_2\text{OH}$ ), and  $\delta=2.61\text{--}2.59$  ppm (m, 2H,  $\text{NCH}_2\text{CH}_2\text{OH}$ ), which confirmed the presence of the expected hydrogen proton (see Fig. 3). The FTIR and  $^1\text{H}$  NMR results indicated that the synthesized product was HOTAAT.

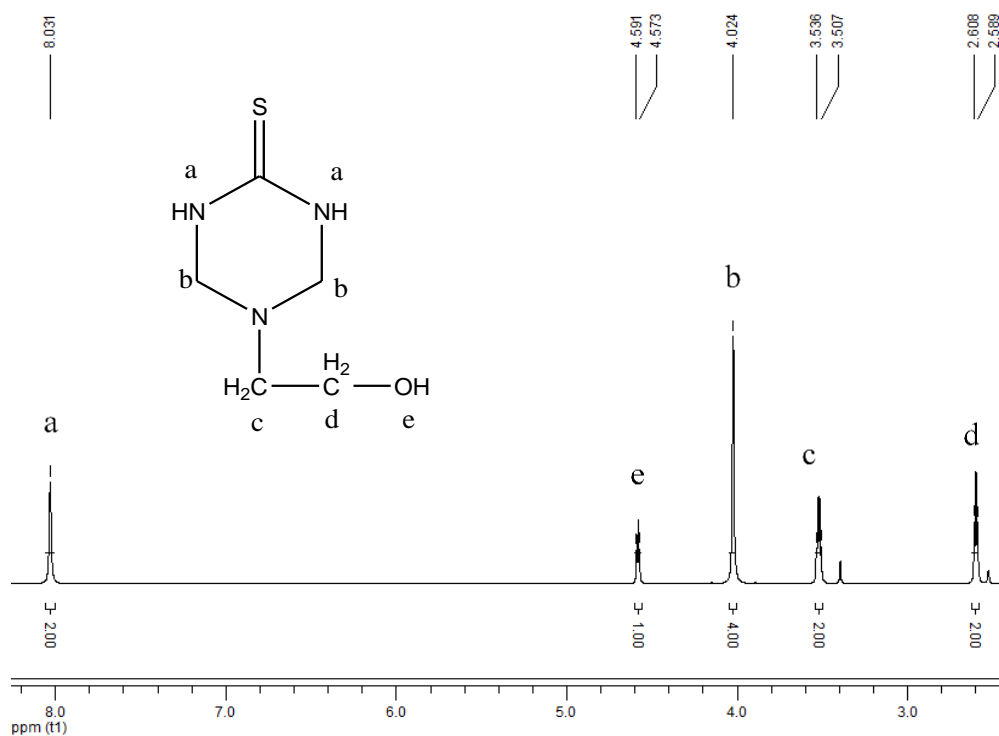


**Figure 3.**  $^1\text{H}$  NMR spectrum of the product

### 3.3. Weight loss measurements

The corrosion inhibition efficiencies of HOTAAT for 10# carbon steel in 2%  $\text{NH}_4\text{Cl}$  solution at different concentrations and temperatures are listed in Table 1.

The corrosion rate of 10# carbon steel in the 2%  $\text{NH}_4\text{Cl}$  solution increased with increasing temperature in the absence of the corrosion inhibitor. As shown in Table 1, HOTAAT exhibited good inhibition performance for 10# carbon steel in the 2%  $\text{NH}_4\text{Cl}$  solution at various temperatures. The corrosion rate of 10# carbon steel in the presence of the inhibitor decreased with increasing concentration and increased with increasing temperature. Increasing the temperature facilitated the desorption of the corrosion inhibitor molecules from the surface of the carbon steel. As a result, the corrosion rate of carbon steel increased with increasing temperature.

**Table 1.** Corrosion inhibition efficiency of HOTAT for 10# carbon steel in  $\text{NH}_4\text{Cl}$  at different concentrations and temperatures

Concentration (mM)	50 °C		60 °C		70 °C		80 °C	
	$v$ (mm/a)	$IE_w$ (%)	$v$ (mm/a)	$IE_w$ (%)	$v$ (mm/a)	$IE_w$ (%)	$v$ (mm/a)	$IE_w$ (%)
0	1.0609	-	1.0861	-	1.4268	-	1.8441	-
0.03	0.5474	48	0.6097	44	0.8832	38	1.2743	31
0.06	0.4201	60	0.4855	55	0.7319	49	1.0493	43
0.09	0.3215	70	0.3921	64	0.5978	58	0.8833	52
0.12	0.2429	77	0.3085	72	0.5265	63	0.8096	56

### 3.4. Potentiodynamic polarization curve

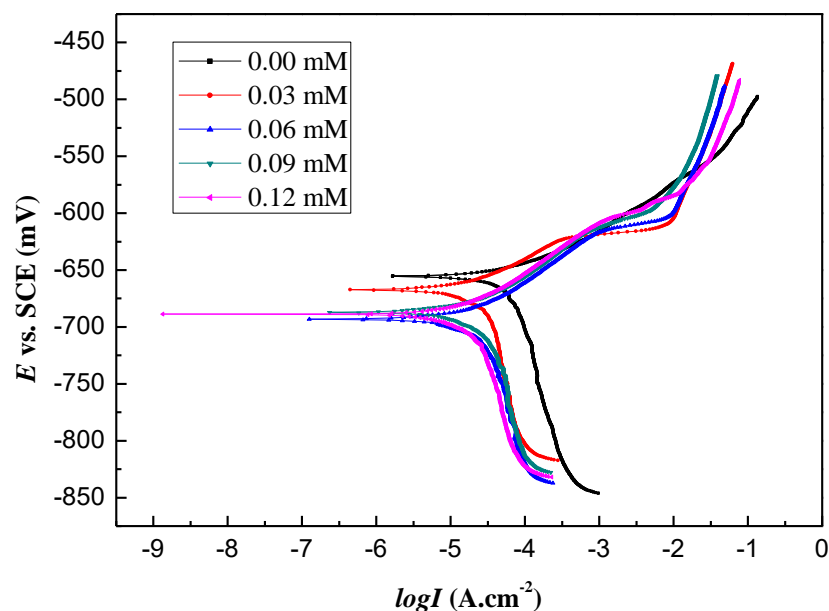
**Figure 4.** Potentiodynamic polarization curves for 10# carbon steel in 2%  $\text{NH}_4\text{Cl}$  solution in the absence and presence of different concentrations of the inhibitor at 50 °C

Fig. 4 shows the potentiodynamic polarization behavior of 10# carbon steel in 2%  $\text{NH}_4\text{Cl}$  solution in the absence and presence of different concentrations of the corrosion inhibitor at 50 °C. The corrosion potential ( $E_{corr}$ ), corrosion current density ( $I_{corr}$ ), and anodic and cathodic Tafel's constant values ( $b_a$  and  $b_c$ , respectively) were calculated from the polarization plots and are summarized in Table 2.

As shown in Table 2, the corrosion current density decreased significantly in the presence of the inhibitor, which indicated that HOTAT is an effective inhibitor of the corrosion of 10# steel. The corrosion potential ( $E_{corr}$ ) decreased slightly in the presence of the inhibitor at all concentrations. The anodic and cathodic Tafel's constant values for 10# steel in 2%  $\text{NH}_4\text{Cl}$  solutions containing the inhibitor varied to some extent. These results indicated that the presence of the inhibitor did not change the corrosion mechanism [36-37]. Both observations suggested that the inhibitor is a mixed-type inhibitor for 10# steel in 2%  $\text{NH}_4\text{Cl}$  solution.

**Table 2.** Potentiodynamic polarization parameters for 10# carbon steel corrosion in 2%  $\text{NH}_4\text{Cl}$  solution in the absence and presence of different concentrations of the synthesized compound at 50 °C

Concentration (mM)	$E_{corr}$ (mV)	$I_{corr}$ (mA cm <sup>-2</sup> )	$-b_c$ (mV dec-1)	$b_a$ (mV dec-1)	$IE_i$ (%)
0.00	-665	0.6897	143.0	33.7	-
0.03	-667	0.3521	187.3	34.3	49
0.06	-693	0.2295	132.5	42.3	67
0.09	-687	0.2209	106.4	45.9	68
0.12	-688	0.1937	181.3	38.9	72

### 3.5. Electrochemical impedance spectroscopy measurements

Electrochemical impedance spectroscopy measurements were used to evaluate the influence of HOTAT on the corrosion behavior of 10# carbon steel in 2%  $\text{NH}_4\text{Cl}$  solution. The Nyquist and Bode plots are shown in Figs. 5 and 6, respectively. The semicircles (Nyquist plot) and low-frequency values of the impedance (Bode plot) obtained in the presence of the inhibitor were higher than those obtained in the blank solution, indicating the good inhibitive behavior of HOTAT.

The equivalent circuit used to fit the electrochemical impedance spectroscopy data is shown in Fig. 7 and is in accordance with other studies [38-39]. The electrochemical impedance spectroscopy parameters determined from the equivalent circuit are shown in Table 3. In Fig. 7 and Table 3,  $R_s$  is the solution resistance. The constant phase element representing the double-layer capacitance ( $C_{dl}$ ) is  $CPE_n$ , and  $R_{ct}$  is the charge transfer resistance. The parameter  $CPE_f$  consists of the film capacitance  $C_f$  and the deviation parameter  $n_1$ . The inhibitive film resistance is denoted  $R_f$ . The values of  $C_{dl}$  and  $C_f$  were calculated using equations (4) and (5) [40-41], respectively:

$$C_f = Y_0^n \cdot R_f^{\frac{1-n}{n}} \quad (4)$$

$$C_{dl} = Y_0^n \cdot \left( \frac{R_s R_{ct}}{R_s + R_{ct}} \right)^{\frac{1-n}{n}} \quad (5)$$

According to these results, the  $R_{ct}$  and  $R_f$  values increased with increasing concentration of the inhibitor. It was proposed that the inhibitor molecules adsorbed on the metal surface, forming a layer that hindered the process of charge transfer [29].

When the inhibitor was added, the  $C_f$  values decreased due to the adsorption of the inhibitor molecules on the metal surface [29, 42-43]. The decreasing trend in the  $C_{dl}$  values indicated that the local

dielectric constant decreased and/or the thickness of the electrical double layer increased due to the formation of a protective layer [44].

The corrosion inhibition efficiency ( $\eta$ ) values were calculated from the electrochemical impedance spectrum using equation (6) [45-46]:

$$\eta = \frac{R_{ct}' - R_{ct}}{R_{ct}} \times 100 \quad (6)$$

where  $R_{ct}'$  and  $R_{ct}$  are the charge transfer resistances of the solution in the presence and absence of the corrosion inhibitor, respectively.

As shown in Table 3, HOTAT exhibited good inhibition performance on 10# carbon steel in 2%  $\text{NH}_4\text{Cl}$  solution. The corrosion inhibition efficiency ( $\eta$ ) increased with increasing concentration of HOTAT.

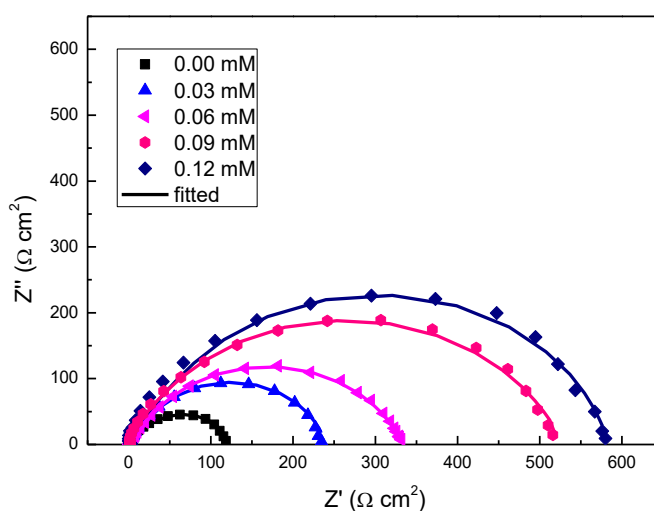


**Figure 5.** Nyquist plots for 10# carbon steel immersed in 2%  $\text{NH}_4\text{Cl}$  solution with and without the inhibitor

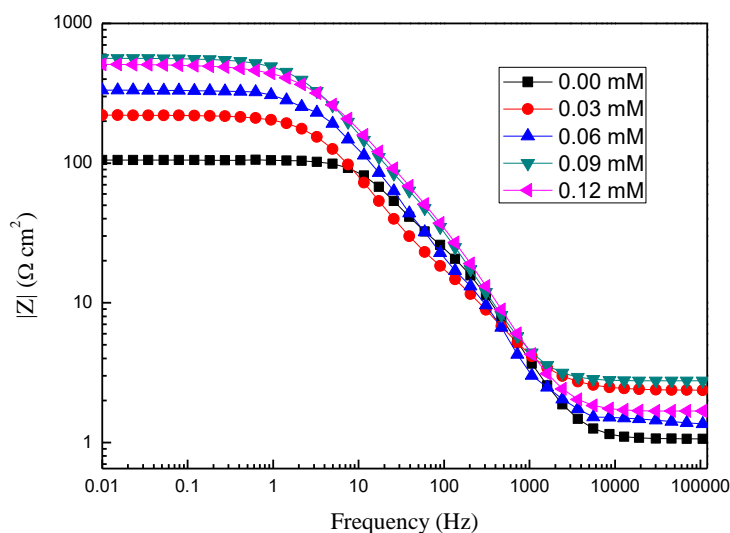


**Figure 6.** Bode plots for 10# carbon steel immersed in 2%  $\text{NH}_4\text{Cl}$  solution with and without the inhibitor

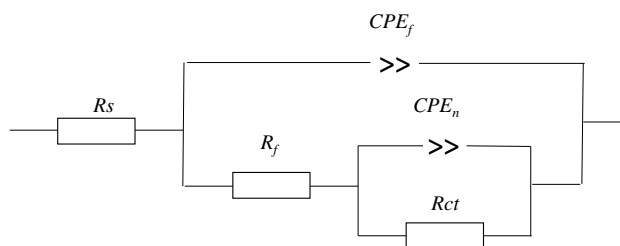


**Figure 7.** Equivalent electrical circuit

**Table 3.** Electrochemical impedance spectroscopy parameters for 10# carbon steel in 2% NH<sub>4</sub>Cl solution without and with the addition of the inhibitor at different concentrations

Inhibitor concentration (mM)	$R_s$ ( $\Omega\text{ cm}^2$ )	$R_f$ ( $\Omega\text{ cm}^2$ )	$R_{ct}$ ( $\Omega\text{ cm}^2$ )	$C_f$ ( $\mu\text{F cm}^{-2}$ )	$n_1$	$C_{dl}$ ( $\mu\text{F cm}^{-2}$ )	$n_2$	$\eta$ (%)
0.00	1.06	28.99	87.83	86.40	1	92.23	0.8	-
0.03	2.35	32.71	207.73	69.96	0.8	67.77	0.8	58
0.06	1.22	55.78	337.62	44.85	1	65.29	0.7	74
0.09	1.68	67.75	460.02	43.02	1	50.64	0.7	81
0.12	2.76	89.41	492.35	38.47	1	26.95	0.8	82

3.6. SEM analysis

The surface morphologies of 10# carbon steel in 2% NH<sub>4</sub>Cl solution at different temperatures are shown in Fig. 8. The surface of the 10# carbon steel was seriously corroded in the 2% NH<sub>4</sub>Cl solution in the absence of the inhibitor at different temperatures (Figs. 8a, b, c and d).

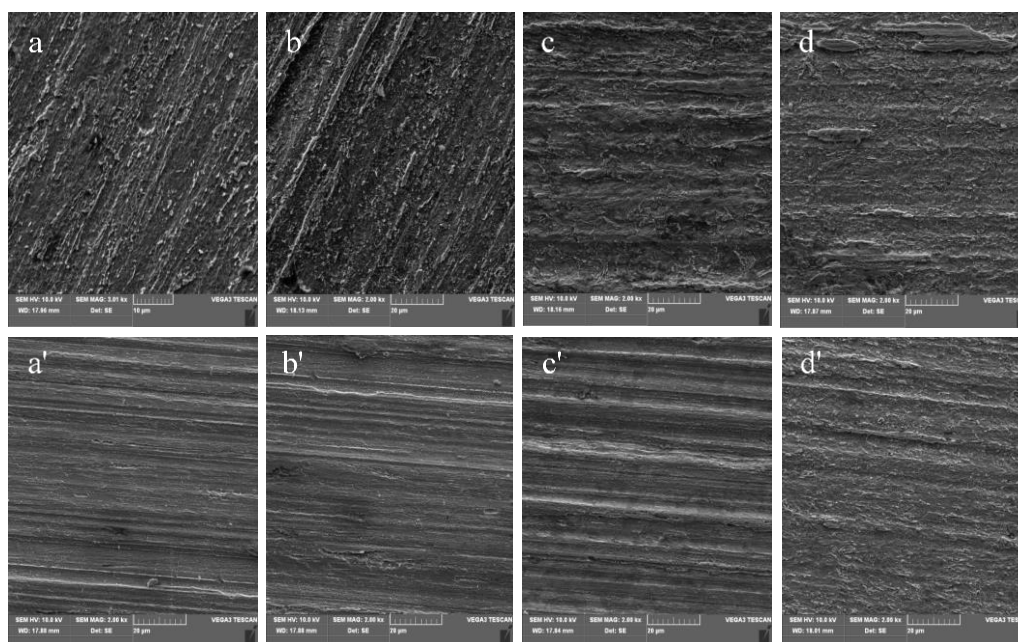


**Figure 8.** Surface morphology of 10# carbon steel in 2% NH<sub>4</sub>Cl solution at different temperatures (a-50 °C, 0.00 mM; a'-50 °C, 0.12 mM; b-60 °C, 0.00 mM; b'-60 °C, 0.12 mM; c-70 °C, 0.00 mM; c'-70 °C, 0.12 mM; d-80 °C, 0.00 mM; d'-80 °C, 0.12 mM)

The samples retrieved from solutions containing the inhibitor had comparatively smoother surfaces (Figs. 8a', b', c' and d') and were only somewhat degraded. However, the surface was less corroded and more uniform at lower temperatures than at higher temperatures, demonstrating the superior anti-corrosion performance of the inhibitor at lower temperatures. The micrographs also confirmed the results of the electrochemical and gravimetric analyses.

### 3.7. Adsorption isotherms

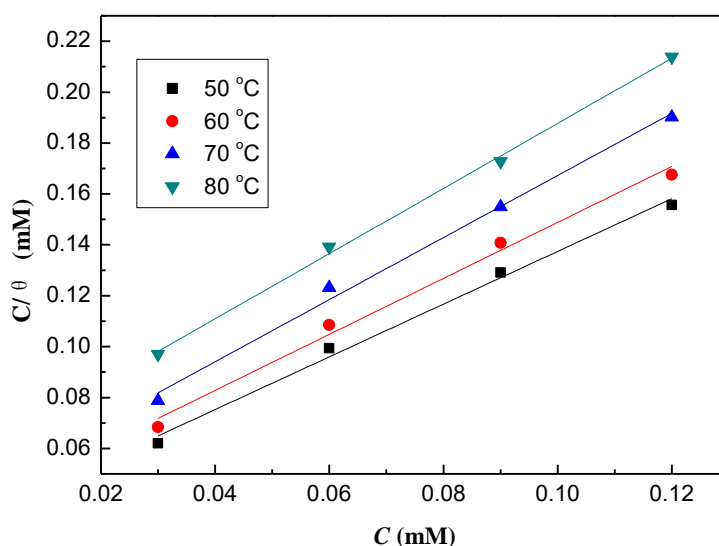
The adsorption isotherm of the corrosion inhibitor describes its adsorption law at a given temperature. It mainly depends on the nature of the corrosion inhibitor itself (polar groups, nonpolar groups, spatial structure) and the metal surface state (non-uniformity). It is generally believed that when the shapes of the anion and anodic polarization curves do not change considerably, the coverage value  $\theta$  of the corrosion inhibitor on the metal surface is equal to the value of the corrosion inhibition rate.

Fig. 9 shows that the plots of  $C/\theta$  vs  $C$  gave straight lines, suggesting that the adsorption of the inhibitor at the 10# carbon steel/ $\text{NH}_4\text{Cl}$  solution interface obeys the *Langmuir* adsorption isotherm, which is described by the following equation [47-49]:

$$\frac{C_{inh}}{\theta} = \frac{1}{K_{ads}} + C_{inh} \quad (7)$$

where  $\theta$  is the surface coverage,  $C_{inh}$  is the inhibitor concentration, and  $K_{ads}$  is the adsorption equilibrium constant.

The adsorption equilibrium constants ( $K_{ads}$ ) at different temperatures were estimated from the intercepts of the straight lines in the  $C_{inh}/\theta$  vs  $C_{inh}$  plots (see Fig. 9) and are reported in Table 4. The  $K_{ads}$  value decreased with increasing temperature, which was attributed to the increasing desorption of the inhibitor from the metal surface.



**Figure 9.** Langmuir adsorption plots for 10# carbon steel in 2%  $\text{NH}_4\text{Cl}$  with different concentrations of the inhibitor at different temperatures

The standard free energy of adsorption ( $\Delta G^{\circ}_{ads}$ ) could be calculated from the adsorption constant ( $K_{ads}$ ) using equation (8) [50-51]:

$$K = \exp\left(-\frac{\Delta G^{\circ}}{RT}\right) / 55.5 \quad (8)$$

The  $\Delta G^{\circ}_{ads}$  values of the inhibitor were negative (Table 4), indicating spontaneous adsorption of the inhibitor on the steel surface. These  $\Delta G^{\circ}_{ads}$  values ranged from  $-38$  to  $-40$  kJ mol $^{-1}$  (Table 4), which indicated that the inhibitor was adsorbed on the mild steel surface as a consequence of physisorption and chemisorption processes [52].

The adsorption heat ( $\Delta H^{\circ}_{ads}$ ) was determined using the van't Hoff equation (equation (9)) [53] and was obtained from the  $\ln K_{ads}$  vs.  $1/T$  slopes (Fig. 10). The negative  $\Delta H^{\circ}_{ads}$  value revealed that the adsorption of the inhibitor was exothermic [54]:

$$\ln K_{ads} = \left(\frac{-\Delta H^{\circ}_{ads}}{RT}\right) + \text{constant} \quad (9)$$

The entropy of the inhibitor adsorption ( $\Delta S^{\circ}_{ads}$ ) was obtained using the following equation [55-56]:

$$\Delta G^{\circ}_{ads} = \Delta H^{\circ}_{ads} - T\Delta S^{\circ}_{ads} \quad (10)$$

The positive  $\Delta S^{\circ}_{ads}$  values (Table 4) were related to the increase in the inhibitor adsorption disorder. This result indicated that the inhibitor molecules adsorbed on the mild steel surface as water molecules desorbed.

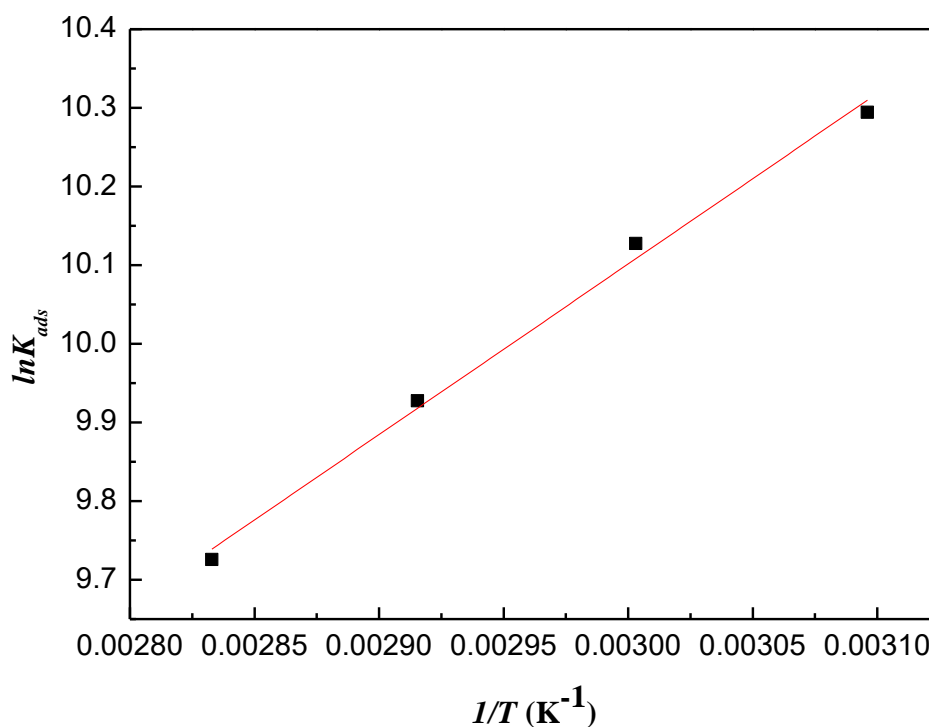


**Figure 10.** The relation between  $\ln K_{ads}$  and  $1/T$  for 10# carbon steel in 2%  $\text{NH}_4\text{Cl}$  solution with different concentrations of the inhibitor at different temperatures

**Table 4.** Standard thermodynamic parameters for the adsorption of the synthesized compound on the 10# carbon steel surface in 2% NH<sub>4</sub>Cl solutions with different inhibitor concentrations at various temperatures

Temperature (°C)	$K_{ads}$	$\Delta G^{\circ}_{ads}$ (kJ mol <sup>-1</sup> )	$\Delta H^{\circ}_{ads}$ (kJ mol <sup>-1</sup> )	$\Delta S^{\circ}_{ads}$ (J mol <sup>-1</sup> K <sup>-1</sup> )
50	29559	-38		63
60	25018	-39	-18	63
70	20488	-40		63
80	16739	-40		63

#### 4. CONCLUSIONS

HOTAT was synthesized, and its corrosion inhibition performance for 10# carbon steel in 2% NH<sub>4</sub>Cl solution was studied by weight loss and electrochemical methods. According to the results, the following conclusions can be drawn:

1. HOTAT was successfully synthesized, and its chemical structure was characterized by FTIR and <sup>1</sup>H NMR.
2. The inhibition efficiency of HOTAT on 10# carbon steel in 2% NH<sub>4</sub>Cl solution increased with increasing inhibitor concentration. Furthermore, HOTAT exhibited mixed-type inhibitor efficiency.
3. The mechanism of corrosion inhibition involved the adsorption of the inhibitor on the 10# carbon steel surface as described by the Langmuir adsorption isotherm.
4. The HOTAT adsorption process was spontaneous and exothermic as revealed by the negative  $\Delta G^{\circ}_{ads}$  and  $\Delta H^{\circ}_{ads}$  values.

#### ACKNOWLEDGMENTS

This study was funded by the Open Foundation of the State Key Laboratory for Performance and Structure Safety of Petroleum Tubular Goods and Equipment Materials and by the Basic Research and Strategic Reserve Technology Research Fund (project of China National Petroleum Corporation (2018Z-01)).

#### References

1. Seyyed Arash Haddadi, Eiman Alibakhshi, Ghasem Bahlakeh, Bahram Ramezanzadeh and Mohammad Mahdavianb, *J. Mol. Liq.*, 284 (2019) 682.
2. M. Mahdavian, A.R. Tehrani-Bagha, E. Alibakhshi, S. Ashhari, M.J. Palimi, S. Farashi, S. Javadian and F. Ektefa, *Corros. Sci.*, 137 (2018) 62.
3. S.K. Saha, A. Dutta, P. Ghosh, D. Sukul and P. Banerjee, *Phys. Chem. Chem. Phys.*, 18 (2016) 17898.
4. Ashish Kumar Singh and M.A. Quraishi, *J. Appl. Electrochem.*, 40 (2010) 1293.
5. Ivana Jevremović, Marc Singer, Srđan Nešić and Vesna Mišković-Stanković, *Corros. Sci.*, 77 (2013) 265.
6. Mónica Corrales-Luna, Tu Le Manh and E.M. Arce-Estrada, *Int. J. Electrochem. Sci.*, 14 (2019) 4420.

7. Adewale Adewuyi, Andrea Göpfert and Thomas Wolff, *Ind. Crop. Prod.*, 52 (2014) 439.
8. Zhihua Tao, Wei He, Shouxu Wang and Guoyun Zhou, *Ind. Eng. Chem. Res.*, 52 (2013) 17891.
9. Pavithra M. Krishnegowda, Venkatarangaiah T. Venkatesha, Punith Kumar M. Krishnegowda and Shylesha B. Shivayogiraju, *Ind. Eng. Chem. Res.*, 52 (2013) 722.
10. A.S. Foudal, M.M. Hegazi and Ali. El-Azaly, *Int. J. Electrochem. Sci.*, 14 (2019) 4668.
11. Mohammad M. Fares, A.K. Maayta and Mohammad M. Al-Qudah, *Corros. Sci.*, 60 (2012) 112.
12. Salawu Abdulrahman Asipita, Mohammad Ismail, Muhd Zaimi Abd Majid, Zaiton Abdul Majid, CheSobry Abdullah and Jahangir Mirzac, *J. Clean. Prod.*, 67 (2014) 139.
13. V.V. Torres, V.A. Rayol, M. Magalhães, G.M. Viana, L.C.S. Aguiar, S.P. Machado, H. Orofino and E. D'Elia. *Corros. Sci.*, 79 (2014) 108.
14. Aprael S. Yaro, Anees A. Khadom and Rafal K. Wael, *Alex. Eng. J.*, 52 (2013) 129.
15. G. Moretti, F. Guidi and G. Grion, *Corros. Sci.*, 46 (2004) 387.
16. Salah Abd El Wanees, Mohamed I. Alahmdi, Abla Ahmed Hathoot and Sabry Shaloot, *Chem. Process Eng. Res.*, 39 (2015) 13.
17. M.A. Quraishi and H.K. Sharma, *J. Appl. Electrochem.*, 35 (2005) 33.
18. Farhat Aisha Ansari and M.A. Quraishi. *Arab. J. Sci. Eng.*, 36 (2011) 11.
19. Sibel Zor, *Prot. Met. Phys. Chem. Surf.*, 50 (2014) 530.
20. Benchikh A, Aitout R, Makhloufi L, Benhaddad L and Saidani B., *Desalination*, 249 (2009) 466.
21. Jasna Halambek, Katarina Berković and Jasna Vorkapić-Furač, *Mater. Chem. Phys.*, 137 (2013) 788.
22. Layla A. Al Juhaiman, Amal Abu Mustafa and Wafaa K. Mekhamer, *Anti-Corros. Method. M.*, 60 (2013) 28.
23. El-Deeb Mohamed M., Ads Essam N. and Humaidi Jamal R., *Int. J. Electrochem. Sci.*, 13 (2018) 4123.
24. Umoren SA, Inam EI, Udoidiong AA, Obot IB, Eduok UM and Kim KW, *Chem. Eng. Commun.*, 202 (2015) 206.
25. Alvisi PP and Lins VDFC, *Eng. Fail Anal.*, 15 (2008) 1035.
26. Toba K, Ueyama M, Kawano K and Sakai J, *Corrosion*, 68 (2012) 1049.
27. Prince Kumar Baranwal and Prasanna Venkatesh Rajaraman, *J. Mater. Res. Technol.*, 8 (2019) 1366.
28. Paulo Pio Alvisi and Vanessa de Freitas Cunha Lins, *Eng. Fail. Anal.*, 15 (2008) 1035.
29. Yujie Qiang, Shengtao Zhang, Lei Guo, Shenying Xu, Li Feng, Ime B. Obot and Shijin Chen, *J. Clean. Prod.*, 52 (2017) 17.
30. M.A. Deyab, *J. Power Sources*, 280 (2015) 190.
31. Saviour A. Umoren, Ime B. Obot, A. Madhankumar and Zuhair M. Gasem, *Carbohydr. Polym.*, 124 (2015) 280.
32. M.R. Noor El-Din and E.A. Khamis, *J. Ind. Eng. Chem.*, 24 (2015) 342.
33. M. Behpour, S.M. Ghoreishi, N. Mohammadi, N. Soltani and M. Salavati-Niasari, *Corros. Sci.*, 52 (2010) 4046.
34. Sudhish Kumar Shukla and M.A. Quraishi, *Mater. Chem. Phys.*, 120 (2010) 142.
35. B.M. Prasanna, B.M. Praveen, Narayana Hebbar and T.V. Venkatesha, *Anti-Corros. Method. M.*, 63 (2016) 47.
36. A Chetouani, A Aouniti, B Hammouti, N Benchat, T Benhadda and S Kertit, *Corros. Sci.*, 45 (2003) 1675.
37. Dileep Kumar Yadav, B. Maiti and M.A. Quraishi, *Corros. Sci.*, 52 (2010) 3586.
38. Francisco Javier Rodríguez-Gomez, Maira Perez Valdelamar, Araceli Espinoza Vazquez, Paulina Del Valle Perezb, Rachel Mata, Alan Miralrio and Miguel Castro, *J. Mol. Struct.*, 1183 (2019) 168.
39. Ambrish Singh, Yuanhua Lin, Wanying Liu, Shijie Yu, Jie Pan, Chengqiang Ren and Deng Kuanhai, *J. Ind. Eng. Chem.*, 20 (2014) 4276.
40. Ambrish Singh, Yuanhua Lin, Mumtaz A. Quraishi, Lukman O. Olasunkanmi, Omolola E. Fayemi,

- Yesudass Sasikumar, Baskar Ramaganthan, Indra Bahadur, Ime B. Obot, Abolanle S. Adekunle, Mwacham M. Kabanda and Eno E Ebenso, *Molecules*, 20 (2015) 15122.
41. B. Hirschorn, M.E. Orazem, B. Tribollet, V. Vivier, I. Frateur and M. Musiani, *Electrochim. Acta*, 55 (2010) 6218.
  42. M. Yadav, T.K. Sarkar and T. Purkait, *J. Mol. Liq.*, 212 (2015) 731.
  43. R.A. Prabhu, T.V. Venkatesha, A.V. Shanbhag, G.M. Kulkarni and R.G. Kalkhambkar, *Corros. Sci.*, 50 (2008) 3356.
  44. E. Alibakhshi, E. Ghasemi and M. Mahdavian, *Corros. Sci.*, 77 (2013) 222.
  45. Mahmoud N. EL-Haddad. Carbohyd, *Polymer*, 112 (2014) 595.
  46. J. Aljourani, K. Raeissi and M.A. Golozar, *Corros. Sci.*, 51 (2009) 1836.
  47. S.A. Abd El-Maksoud and A.S.Fouda, *Mater. Chem. Phys.*, 93 (2005) 84.
  48. P. Mohan, G. Paruthimal Kalaignan, *J. Mater. Sci. Technol.*, 29 (2013) 1096.
  49. Muzaffer Özcan, Ramazan Solmaz, Gülfeza Kardaş and İlyas Dehri, *Colloid. Surface. A*, 325 (2008) 57.
  50. L. Fragoza-Mar, O. Olivares-Xometl, M.A. Domnguez-Aguilar, E.A. Flores, P. Arellanes-Lozada and F. Jiménez-Cruz, *Corros. Sci.*, 61 (2012) 171.
  51. A.O. Yuce and G. Kardas, *Corros. Sci.*, 58 (2012) 86.
  52. X. Wang, H. Yang and F. Wang, *Corros. Sci.*, 55 (2012) 145.
  53. M.A. Hegazy, E.M.S. Azzam, N.G. Kandil, A.M. Badawi and R.M. Sami, *J. Surfactants Deterg.*, 19 (2016) 861.
  54. H.M. Abd El-Lateef, V.M. Abbasov, L.I. Aliyeva, E.E. Qasimov and I.T. Ismayilov, *Mater. Chem. Phys.*, 142 (2013) 502.
  55. Sh. Pournazari, M.H. Moayed and M. Rahimizadeh, *Corros. Sci.*, 71 (2013) 20.
  56. G. Moretti, F. Guidi and F. Fabris, *Corros. Sci.*, 76 (2013) 206.